ADVANCED HEALTHCARE MATERIALS
www.advhealthmat.de

A Rapid and Ultrasensitive Thrombin Biosensor Based on a Rationally Designed Trifunctional Protein

Huayue Zhang, Lu Yang, Xiaqing Zhu, Yanyan Wang, Haitao Yang, and Zefang Wang**

Rapid and sensitive detection of thrombin is imperative for the early diagnosis, prevention, and treatment of thrombin-related diseases. Here, an ultrasensitive and rapid thrombin biosensor is developed based on rationally designed trifunctional protein HTs, comprising three functional units, including a far-red fluorescent protein smURFP, hydrophobin HGFI, and a thrombin cleavage site (TCS). smURFP is used as a detection signal to eliminate any interference from the autofluorescence of sample matrix to increase detection sensitivity. HGFI serve as an adhesive unit to allow rapid immobilization of HTs on a multiwall plate. The TCS linking HGFI and smURFP function as a sensing element to recognize and detect thrombin. HTs immobilization is symmetrically optimized and characterized. Thrombin assay reveals the specific recognition of active thrombin in samples and the hydrolysis of the immobilized HTs, resulting in a decrease in the fluorescence intensity of the sample in a thrombin concentration-dependent manner. The limit of detection (LOD) is as low as 0.2 aM in the serum. To the authors' knowledge, this is the lowest LOD ever reported for any thrombin biosensor. This study sheds light on the engineering of multifunctional proteins for biosensing.

1. Introduction

Thrombin is a serine protease generated from the proteolytic activation of prothrombin and is known to modulate blood coagulation in humans through the conversion of soluble fibrinogen into insoluble fibrin.[1] Thrombin is not only associated with bleeding or thrombosis[2] but also with some serious diseases such as Alzheimer's disease,[3] nephrotic syndrome,[4] atherosclerosis,[5] and tumor growth and metastasis.[6] Therefore, it is imperative to design a sensitive, specific, and rapid assay for the detection of thrombin for the early prevention, control, and management of thrombin-related diseases.

Considering the detection principle, the existing thrombin sensing methods may be classified into two groups, namely, the direct and indirect method. While the direct method detects the cleavage activity of thrombin itself,[7] the indirect method does not involve thrombin activity detection but is based on the use of thrombin recognition parts as sensing elements to build-up detection systems.[8] In either case, the measurable detection signal is deemed important to construct thrombin sensing systems. Efforts have been directed to develop detection signals, including fluorescence,[9] colorimetry,[10] and electrochemical-based approaches,[11] of which the fluorescence method is the most commonly sorted strategy owing to the advantages of high sensitivity and ease of operation. However, the excitation wavelength range of conventional fluorophores is generally between 400 and 600 nm.[12] Therefore, the background fluorescence produced by the sample and reaction vessel may severely affect the limit of detection (LOD) when conventional fluorophores are used.

Several studies have successfully demonstrated the improvement in detection sensitivity following autofluorescence reduction in various diseases,[13] but only a few reports have tried addressing the autofluorescence limitation during thrombin detection. In 2013, a time-resolved fluorescence detection system was employed to eliminate the short lifetime autofluorescence in an aptamer-directed thrombin assay.[14] In 2018, Xiong et al. developed phosphorescent quantum dots with long lifetime to eliminate autofluorescence in their phosphorescence resonance energy transfer system.[15] Although the above-mentioned methods solved the problem of autofluorescence to a certain extent, the complexity of the sensor design and requirement for testing equipment limit their applications. Herein, we describe the development of a biosensor based on a rationally designed trifunctional fusion protein that was effective in reducing autofluorescence to facilitate rapid and convenient detection of thrombin.

Our fusion protein sensor comprises three parts, namely a detection signal, an adhesive part, and a sensing element. smURFP, a novel small ultra-red fluorescent protein with absorption and emission maxima of 642 and 670 nm, respectively, was used as the detection signal.[16] The degradation half-life of smURFP is about 17 h, suggestive of its photostability. Moreover, smURFP

H. Zhang, L. Yang, X. Zhu, Prof. Y. Wang, Prof. H. Yang, Prof. Z. Wang
School of Life Sciences
Tianjin Key Laboratory of Function and Application of Biological Macromolecular Structures
College of Precision Instrument and Opto-Electronics Engineering
Tianjin University
Tianjin 300072, China
E-mail: yanyanwang@tju.edu.cn; zefangwang@tju.edu.cn
Prof. H. Yang, Prof. Z. Wang
Center for Anti-Infective Research & Development
Tianjin International Joint Academy of Biotechnology and Medicine
Tianjin 300457, China

The ORCID identification number(s) for the author(s) of this article can be found under https://doi.org/10.1002/adhm.202000364

DOI: 10.1002/adhm.202000364

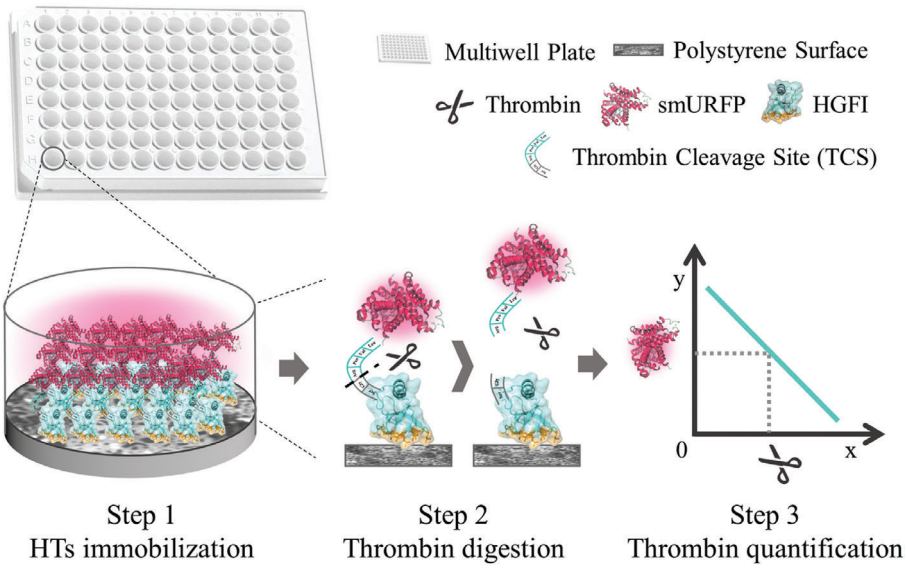

Figure 1. Schematic diagram of thrombin detection workflow.

has an extremely large extinction coefficient (180 000 M^{-1} cm^{-1}) that makes its signal comparable to that of eGFP. It is about twofold brighter than most red or far-red fluorescent proteins derived from coral.[17] These unique properties of smURFP make it an ideal detection signal to eliminate any autofluorescence interference in our sensing system.[18] Hydrophobin HGFI was used as the adhesive part, and could easily immobilize the fusion protein onto multiwall plates via self-assembly. Hydrophobin, a small secreted protein produced by filamentous fungi, is capable of forming self-assemblies on different interfaces.[19] Self-assembled hydrophobin on substrates can be used to immobilize proteins.[20] The specific thrombin cleavage site (TCS; LVPR/GS) was used as the sensing element and served as a linker between HGFI and fluorescent protein. As a result, the intensity of the fluorescent signal on the surface of multiwall plates changed depending on the concentration of thrombin. The sensing mechanism of our biosensor relies on the ability of active thrombin in samples to specifically recognize and hydrolyze its cleavage site in the fusion protein, resulting in a subsequent decrease in the fluorescence intensity of the sample (**Figure 1**).

With this trifunctional protein assembly, we systematically built-up a novel far-red fluorescence-based biosensor to detect thrombin in the serum. Our results show that this biosensor facilitates the rapid and ultrasensitive detection of thrombin in 20 min. The LOD value was as low as 0.2 aM for serum samples. To the best of our knowledge, this is the lowest LOD ever reported for any thrombin biosensor. We also obtained a wide linear range from 1.07 aM to 0.01 mM, which is among the best obtained range for thrombin assay.

2. Results and Discussion

2.1. Production and Characterization of HTs

Figure 2a shows the three components employed to design the multifunctional fusion protein of the thrombin-detecting sensor. The first component is hydrophobin HGFI, in which the yellow part represents a hydrophobic patch comprising hydrophobic residues on the protein surface. This unique structure facilitates the self-assembly of hydrophobin on different interfaces and imparts it with the property of "adhesive binding" for immobilization of fusion proteins.[21] The second component is the TCS, which serves as a "sensing element" in our biosensor. We chose Leu-Val-Pro-Arg-Gly-Ser as the site for thrombin digestion that has been widely used for thrombin detection.[7,22] This consensus sequence is specifically recognized by thrombin and has better cutting efficiency than other thrombin digestion sites.[7] A far-infrared fluorescent protein smURFP was the third part used as the detection signal in our biosensor. smURFP is expected to avoid the autofluorescence from sample matrix and reaction vessel, consequently increasing the LOD of our biosensor. The fusion protein was produced using a synthetic biology method (Figure S1, Supporting Information) and termed as HTs (Figure 2b). Recombinant HTs was then expressed in an *Escherichia coli* expression system. Figure 2c shows the result of size-exclusion chromatography for HTs. Fractions corresponding to the predominant peak were lyophilized and analyzed by sodium dodecyl sulfate polyacrylamide gel electrophoresis (SDS-PAGE). Single bands indicated the high purity of recombinant HTs obtained after purification.

The biological activity of HTs was systematically investigated. In general, all the three components of recombinant HTs are expected to retain their original activities after expression and purification. We verified the fluorescence properties of HTs (Figure 2d) and found that the absorption spectrum comprised a major peak at 642 nm, while the emission spectrum displayed a maximum peak at 670 nm wavelength. The absorption and emission spectra of HTs were almost identical to those of native smURFP, confirming the detection signal of HTs. Given that hydrophobin can form an amphiphilic protein-membrane connection via self-assembly to reverse the hydrophilic–hydrophobic property of any surface, the self-assembly of HTs was evaluated

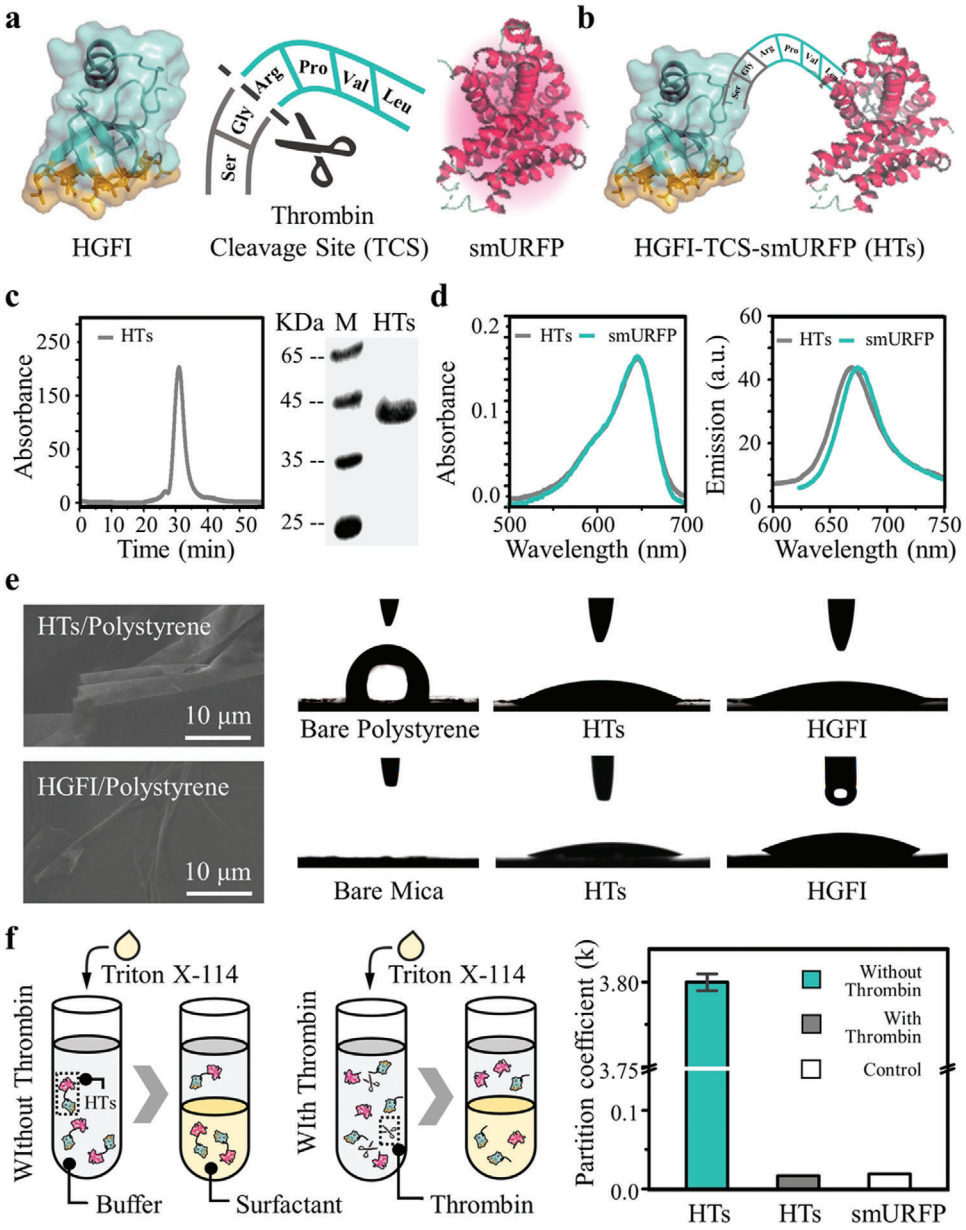

Figure 2. Production and characterization of HTs. a) Components of thrombin sensor. The yellow part of the figure represents a hydrophobic patch comprising hydrophobic residues that allow modification of different interfaces in response to the change in hydrophilic and hydrophobic properties. The scissor represents thrombin. b) The structure diagram of the thrombin detection sensor HTs. c) Results of size-exclusion chromatography and SDS-PAGE of HTs. d) Absorption and emission spectra of HTs and smURFP. e) SEM images of self-assembled HTs film and native HGFI film and WCA measurements of polystyrene and mica before and after modification with HTs and HGFI. f) Schematic diagram of ATPS and determination of the change in the partition coefficient of the fluorescent protein ($n = 3$).

by water contact angle (WCA) measurement at both the hydrophobic and hydrophilic surfaces.[20d] Before WCA measurement, scanning electron microscopy (SEM) was performed to confirm the self-assembly of HTs to form a protein film on surfaces. Figure 2e shows a self-assembled HTs film on the polystyrene surface with the wrinkles or folds like native HGFI. We performed WCA measurement and found that polystyrene had a typical hydrophobic property (WCA is 108.1°), and mica sheet displayed obvious hydrophilicity (WCA is 2°). In contrast, the surface properties of both polystyrene and mica significantly changed after modification with HTs. The WCA of HTs-modified polystyrene sharply decreased from 108.1° to 39.4°. Several studies have shown that the self-assembly of amphiphilic hydrophobin on any hydrophobic surface results in the adherence of the "hydrophobic patch" exposed on hydrophobin surface onto the hydrophobic surface via strong hydrophobic interactions.[23] Thus, the hydrophilic part of hydrophobin was exposed, resulting in the transformation of the hydrophobic surface into a hydrophilic one.[24] The WCA of the HTs-modified mica sheet increased from 2° to 23°. These results indicate that HTs retained

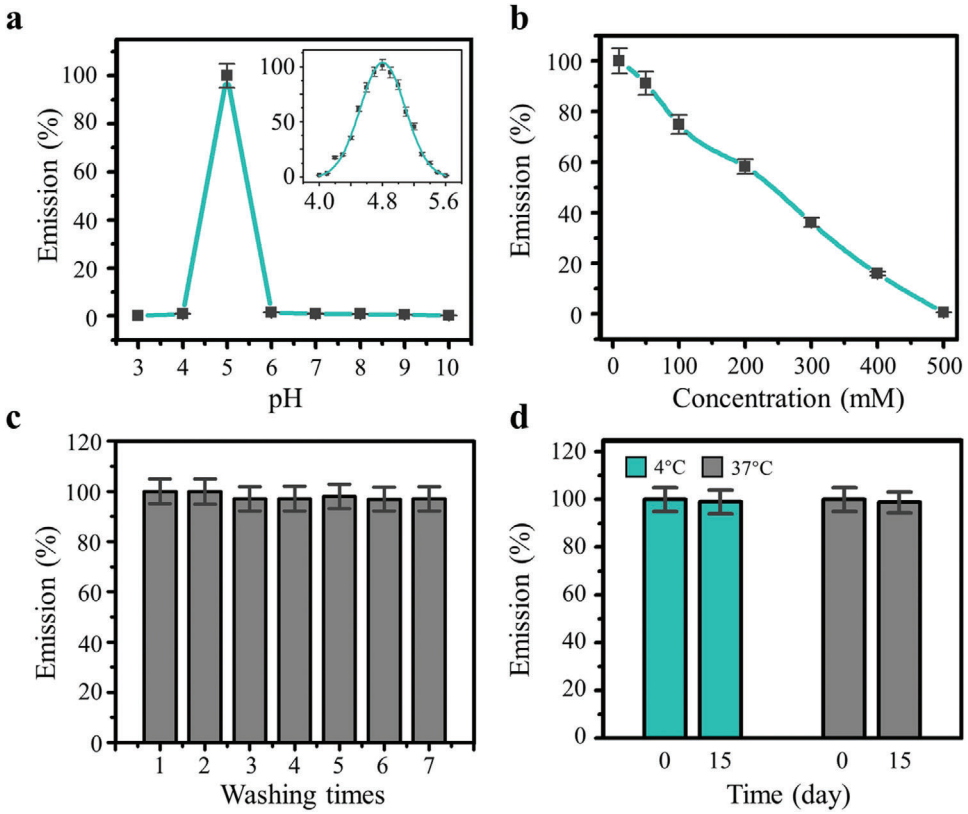

Figure 3. Optimization of the protocol for the immobilization of HTs onto multiwell plates. a) The effect of pH (3–10) on the adsorption of HTs ($n = 3$). b) The effect of different NaCl concentrations (10–500 mM) on the adsorption of HTs ($n = 3$). c) Verification of the wash-resistant property of immobilized HTs following washing with 10 mM NaH_2PO_4-NaOH buffer (pH, 7.4) ($n = 3$). d) The 15-day stability of the fluorescence intensity of immobilized HTs at different temperatures (4 and 37 °C; $n = 3$).

its ability to self-assemble and could be used to modify different interfaces, consistent with the function of native hydrophobin.

The biological function of the TCS used as the "sensing element" was verified. Native hydrophobin exhibits an extremely strong separation behavior in an aqueous two-phase system (ATPS) owing to its amphiphilic nature.[25] As we proved that HTs could behave like native hydrophobin, we used an ATPS to verify the effectiveness of the TCS. Most intact HTs without thrombin cleavage should theoretically move to the lower phase of the ATPS in the presence of the surfactant Triton X-114 because of the partition effect of hydrophobin. If the TCS of HTs is still functional, hydrophobin HGFI and smURFP may separate after the addition of thrombin to the HTs solution. As a consequence, most smURFP tended to get distributed into the upper phase of the ATPS with the removal of hydrophobin HGFI. Partition coefficient describes the ratio of the concentration of smURFP protein between the lower surfactant phase and the upper buffer phase. As shown in Figure 2f, the partition coefficient value for smURFP was about 3.8 in the absence of thrombin, suggesting that most HTs containing smURFP was present in the lower surfactant phase. In contrast, the partition coefficient of the fluorescent protein reduced to about 0.02 after the addition of thrombin, consistent with the original partition coefficient of smURFP in the ATPS. These results indicate that the TCS was functional and was recognized and cleaved by thrombin, resulting in the movement of the separated smURFP into the upper phase of the ATPS. In summary, the multifunctional protein HTs was accurately produced and ready for sensor construction.

2.2. Optimizing the Immobilization of HTs onto the Multiwell Plates

After the successful construction of the fusion protein HTs, we designed the biosensor. The first step for sensor construction was immobilization of HTs onto the surface of a multiwall plate, which was made of polystyrene. In our previous study, we found that the physical adsorption of hydrophobin on different interfaces was strongly affected by several conditions, including pH and salt concentration.[26] Therefore, we systematically investigated the effects of these factors on the adsorption of HTs on multiwell plates. As shown in Figure S2, Supporting Information, HTs had a stable fluorescence under all tested conditions, suggesting that both pH and salt concentration had negligible effects on HTs fluorescence. Therefore, the fluorescence intensity of HTs was used as the indicator to quantify the result of adsorption. As shown in **Figure 3**a, the adsorption of HTs was greatly affected by pH. Maximum binding was achieved at pH 5, which was slightly below the calculated pI of HTs (pI = 5.3). We carefully

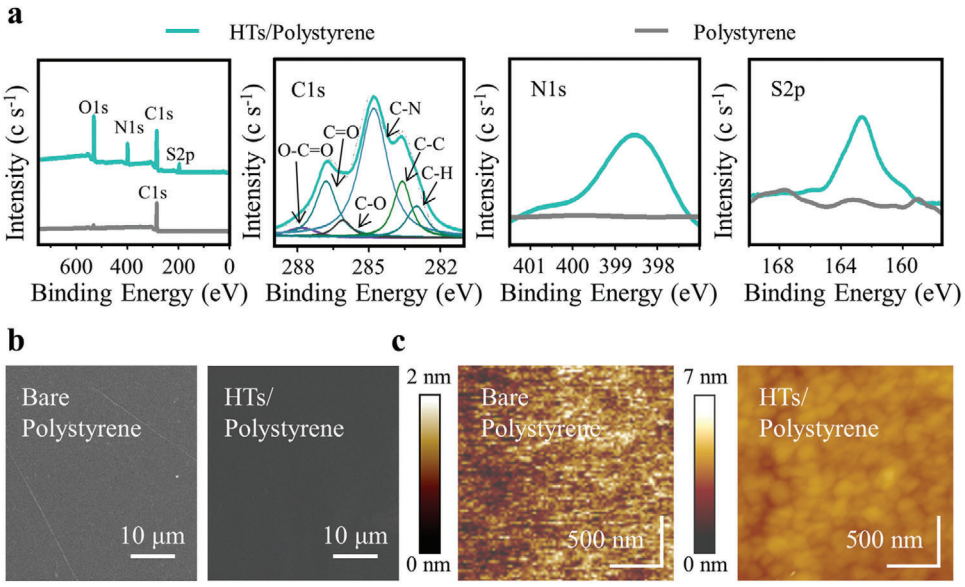

Figure 4. Characterization of HTs-modified multiwall plates. a) Wide XPS spectra of HTs/polystyrene and bare polystyrene, and high-resolution spectra of C1s, S2p, and N1s. b) SEM images of bare polystyrene and self-assembled HTs film on polystyrene surface. c) AFM images of bare polystyrene and self-assembled HTs film on polystyrene surface.

titrated the adsorption of HTs on the multiwell plate around pH 5 and found it (inserted panel in Figure 3a) to sharply decreased as the pH value shifted away from 4.8. For instance, a change of about 1 pH unit resulted in almost complete loss of the binding between HTs and the multiwell plate. Therefore, the optimal pH for HTs adsorption was determined to be 4.8. These results were consistent with our previous finding that the maximum adsorption of native hydrophobin on hydrophobic surfaces is achieved around the pI value of hydrophobin.

Salt concentration is a crucial factor that controls the adsorption of native hydrophobin on hydrophobic surfaces.[26] Salt contributes to the adsorption of the fusion protein HTs on the hydrophobic surface of multiwell plate (Figure 3b). The maximum binding of HTs was achieved at low salt concentrations. As the ionic strength increased, the binding of HTs rapidly decreased. Hence, all the following HTs binding experiments were performed at a low (10 mM) salt concentration. Finally, the stability of the immobilized HTs was examined under different conditions. The bound HTs underwent several rounds of washing during the whole experiment. Therefore, we washed the multiwell plate to verify its binding strength with HTs. Figure 3c shows that the fluorescence intensity of HTs remained unchanged after seven rounds of washing using the buffer employed in the construction of our biosensor. This result indicates that the interaction between the immobilized HTs and polystyrene substrate was rather strong. Wash-resistant binding of immobilized HTs is advantageous for the construction of our biosensor. We also confirmed the stability of the immobilized HTs under defined storage conditions. As shown in Figure 3d, the fluorescence intensity was rather stable during the 15 day storage period at 4 and 37 °C. These results reveal the long-time stability of the fluorescence intensity of immobilized HTs at different temperatures. Thus, we demonstrate the fluorescence stability of HTs that was unaffected by the immobilization process.

2.3. Characterization of HTs-Modified Multiwall Plate

To confirm the immobilization and self-assembly of HTs onto the surface of polystyrene, the chemical composition of the polystyrene surface before and after HTs deposition was analyzed using X-ray photoelectron spectroscopy (XPS) (**Figure 4**a). The complete XPS spectra revealed the overall changes in the O1s, N1s, C1s, and S2p of bare polystyrene and HTs-modified polystyrene. A typical C1s (284.1 eV) element signal was recorded in the wide XPS spectra of bare polystyrene. The intensity of C1s elemental peak of HTs-modified polystyrene decreased. Moreover, the C1s high-resolution XPS peaks of HTs-modified polystyrene could fit into six components at 283.0 (C–H), 283.6 (C–C), 284.8 (C–N), 286.1 (C–O), 286.8 (C O), and 287.8 eV (O–C O). These species were all expected from the molecular structure of HTs, indicative of the self-assembly and deposition of HTs on the surface of polystyrene. In addition, high intensities of N1s (398.5 eV) and S2p (162.5 eV) observed in the high-resolution XPS spectra of HTs-modified polystyrene revealed the adsorption of HTs on the surface of polystyrene.

We performed SEM to observe morphological changes on polystyrene surface before and after HTs modification. As shown in Figure 4b, the surface of polystyrene was relatively flat, but long ridges crossing the surface were observed. After HTs modification, the long ridges disappeared and the surface became obviously smoother. The change in surface morphology indicated the self-assembly of HTs onto the polystyrene surface. We occasionally observed the obvious folded membrane structures at the edge of HTs-modified polystyrene (Figure S3, Supporting Information). Hydrophobin can self-assemble into elastic films on different interfaces.[27] Therefore, these results strongly confirm the self-assembly of HTs into the membranes on polystyrene surface. The morphological changes on polystyrene surface before and after HTs modification were also investigated by atomic force

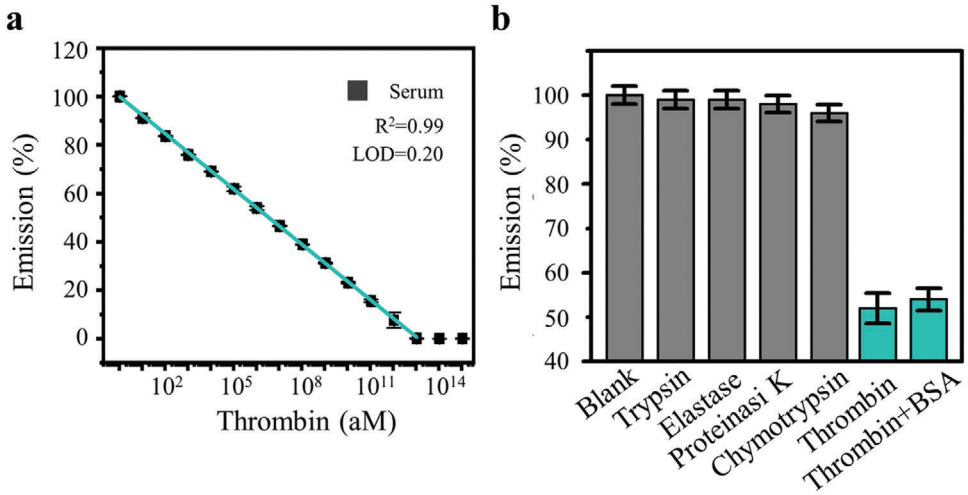

Figure 5. Thrombin assay. Detection curve that simulates the actual detection situation and specificity of the assay. a) Logarithmic plot of the detection curve of the fluorescence emission of 0.4 mg mL^{-1} HTs at 670 nm versus thrombin concentration in the serum at pH 7.4 ($n = 3$). b) Percentage (%) of the fluorescence intensity of HTs in the presence of 10^7 aM of different proteases (trypsin, elastase, chymotrypsin, proteinase K, thrombin, and 3 μM BSA along with thrombin) ($n = 3$).

microscopy (AFM). Figure 4c shows that bare polystyrene displayed a smooth surface with a root mean square roughness (R_q) of 1.38. In contrast, a protein layer was formed on HTs-modified polystyrene surface that resulted in an increase in the R_q value to 3.26 (Figure S3, Supporting Information). As shown in Figure 4a, bare polystyrene was quite smooth but covered with HTs molecules following HTs treatment. The average height of the adsorbed HTs molecules was about 7 nm (averaged from three representative heights 6.6 nm, 7.1 nm, and 7.3 nm in Figure S4b, Supporting Information). Considering the theoretical height of HTs (in the range of 6.1–9.3 nm, as calculated from the 3D structures of HGFI and smURFP; Figure S5, Supporting Information), we propose that a protein monolayer was formed on the HTs-modified polystyrene surface. In this protein monolayer, the adhesive part hydrophobin HGFI could immobilize the whole HTs protein on the polystyrene substrate leaving the TCS and the reporter smURFP exposed to the solvent.

2.4. Thrombin Assay

Before we performed the assay, HTs was immobilized on the surface of the multi-well plate under optimized conditions. Serum samples containing different concentrations of thrombin were added to HTs-immobilized 96-well plates to obtain a standard curve. As expected, the fluorescence intensity of HTs decreased owing to the cleavage of the smURFP probe from the fusion protein with an increase in the concentration of thrombin. To demonstrate the change in the fluorescence intensity in a range of several orders of magnitude, the results were reported on a logarithmic scale. A linear trend was observed in the whole concentration range of thrombin (**Figure 5**a) when the concentration of HTs was 0.4 mg mL^{-1}. Higher concentrations of fusion protein showed a non-linear trend probably owing to the formation of a multi-protein layer on the polystyrene surface, as seen by AFM (Figure S6, Supporting Information). The linear equation

$$y = a + b \log x \quad (1)$$

was used to fit the data on HTs fluorescence and thrombin concentration (a and b represent the intercept and slope, respectively).

According to the $3S_b/m$ criterion (m is the slope of the curve; S_b is the standard deviation of the blank), the LOD was 0.2 aM. To the best of our knowledge, this is the lowest LOD ever reported for any thrombin biosensor. As shown in Figure S7, Supporting Information, the LOD obtained with buffer was 0.02 aM. This result indicates that the serum matrix had no impact on the detection performance of our biosensor. In addition, we obtained a rather wide linear range between 1.07 aM and 0.01 mM, which is among the best reported range for thrombin assays. We also compared our results with the LOD and linear range of other analytical methods used for thrombin detection (**Table 1**). It is clear that our method serves as a rapid and ultrasensitive fluorescence strategy with the best LOD and a wide linear range to detect thrombin. It also eliminates the need for complex experimental procedures and can effectively avoid interference from the autofluorescence of biological samples. Therefore, the excellent far-infrared characteristics of the probe smURFP along with the high efficiency of the immobilization strategy may contribute to these remarkable results.

The specificity of this thrombin detection system was tested by evaluating the effect of other proteases. An obvious decrease in the fluorescence intensity was observed only in the presence of thrombin (Figure 5b), while other proteases failed to induce any change in fluorescence intensity. Moreover, the addition of bovine serum albumin (BSA) to test samples had no effect on the cleavage specificity of the assay. Thus, our method could specifically detect thrombin activity in the serum.

We performed the thrombin assay by adding different concentrations of thrombin to healthy human serum with the standard

Table 1. Comparison of the analytical performances of recent works for thrombin detection.

Detection method	Detection range	LOD (serum)	References
A rationally designed trifunctional protein	1.07 aM–0.01 mM	0.2 aM	Our results
Unmodified gold nanoparticle probes based aptasensor	0–167 nM	—	[28]
Fluorescence resonance energy transfer (FRET) aptasensor	62.5–187.5 pM	pM	[29]
Label-acquired magnetorotation	1–20 nM	—	[30]
Surface plasmon resonance	10 nM	0.1 nM	[31]
A green fluorescent protein based biosensor	aM–mM	2.3 aM	[22]
Label-free and reagentless capacitive aptasensor	10 pM-10 M	16 pM	[32]
Aptamer-based hook-effect-recognizable three-line lateral flow biosensor	1 nM–100 μM	—	[10a]
Aptamer-linked magnetic nanoparticle and redox boundary chip	0.05 nM–0.5 nM	—	[33]
Surface plasmon resonance and quartz crystal microbalance sensors	1 aM–0.1 pM	—	[34]

Table 2. Recovery tests for thrombin in human serum samples. Each sample was analyzed using our proposed biosensor and all values were obtained as an average of three repetitive determinations ± standard deviation (mean ± SD).

Sample	Added [pM]	Found [pM]	Recovery [%]	Relative error [%]
1	5×10^{-7}	$(4.82 \pm 0.12) \times 10^{-7}$	96.40	−3.60
2	5×10^{-6}	$(5.16 \pm 0.06) \times 10^{-6}$	103.20	3.20
3	5×10^{-5}	$(5.23 \pm 1.32) \times 10^{-5}$	104.60	4.60
4	5×10^{-4}	$(5.11 \pm 0.37) \times 10^{-4}$	102.20	2.20
5	5×10^{-3}	$(5.06 \pm 0.16) \times 10^{-3}$	101.20	1.20
6	0.05	0.0492 ± 0.0025	98.40	−1.60
7	0.5	0.496 ± 0.013	99.20	−0.80
8	5	5.04 ± 0.45	100.80	0.80
9	50	49.86 ± 3.76	99.72	−0.28
10	500	497.25 ± 8.21	99.45	−0.55
11	5×10^{3}	$(5.12 \pm 0.03) \times 10^{3}$	102.40	2.40
12	5×10^{4}	$(5.03 \pm 0.11) \times 10^{4}$	100.60	0.60

addition method. As shown in **Table 2**, the recovery value ranged from 96.4% to 104.6% at concentrations from 5×10^{-7} to 5×10^{4} pM, indicative of appropriate thrombin detection in biological samples. Thus, this biosensor can be potentially useful for clinical applications.

3. Conclusion

Here, we demonstrate the development of a fast and ultrasensitive fluorescent system for thrombin detection based on a triple-functional protein HTs. The intentional use of a far-infrared fluorescent protein smURFP avoided interference from the autofluorescence of biological samples and increased the sensitivity of the detection system. The use of hydrophobin enhanced the immobilization efficiency of our fusion protein in a simple and efficient way. Our data show that the strategies used were efficient, as the LOD and linear range of our biosensor were comparable to those of other reported sensors. Our method is robust and reliable for the detection of thrombin in biological samples. The flexibility of our detection system may highlight its potential application for the detection of various other proteases by simply replacing the cleavage linker, which links hydrophobin and fluorescent proteins.

4. Experimental Section

Materials: The coding sequences of HGFI, smURFP, and HO-1 were codon-optimized (Table S1, Supporting Information) and synthesized from GENEWIZ (Tianjin, CHINA). Primers used for gene amplification and overlap polymerase chain reaction (PCR) containing thrombin restriction sites and ribosome binding sites (RBS) were synthesized from GENEWIZ (Tianjin, CHINA). Thrombin, trypsin, elastase, proteinase K, chymotrypsin, and Triton X-114 were purchased from Sigma-Aldrich (Saint Louis, Missouri, USA), while sodium acetate, Tris-HCl, imidazole, sodium chloride (NaCl), peptone, and yeast extract were obtained from Sangon Biotech (Shanghai, CHINA). *E. coli* strains DH5a and BL21 (DE3) and the pET-28a vector were preserved at the Tianjin University (Tianjin, China). T4 DNA ligase, Taq DNA polymerase, all restriction enzymes, and DNA molecular mass markers were procured from Thermo Fisher Scientific (Beijing, CHINA). Deionized water (Millipore Milli-Q grade) with a resistivity of 18.2 MΩ cm was used throughout this study.

Vector Construction: The coding sequences of HGFI, TCS, smURFP, and RBS (5′-*gaattccatcatcaccatcaccattgaaagaaggagatatacatacccc*-3′) were amplified by PCR and linked using overlap PCR. The resulting DNA fragment was gel-purified using a highly pure PCR product purification kit and subjected to restriction digestion using *Bam*HI and *Xho*I. The product was ligated into the corresponding sites of the pET28a vector. The obtained expression vector was introduced into *E. coli* BL21 (DE3) for protein expression.

Expression and Purification of the Trifunctional Protein: *E. coli* BL21 (DE3) colonies were picked up from a Luria Bertani (LB) solid medium plate and grown in 5 mL LB liquid medium (10 g L^{-1} peptone, 10 g L^{-1} NaCl, 5 g L^{-1} yeast extract) at 37 °C and 220 rpm on a rotary shaker for overnight. The culture was then diluted at a ratio of 1:200 using fresh medium and grown up to 0.6 OD (37 °C and 220 rpm). After the temperature of the medium dropped to 16 °C, 500 μM of 1 M isopropyl β-d-1-thiogalactopyranoside (IPTG) was added to induce protein expression at 16 °C and 220 rpm on a rotary shaker for 14–16 h. The cells were sedimented by centrifugation at 4000 rpm and 4 °C for 25 min, resuspended in Tris buffer A (50 mM Tris, 300 mM NaCl [pH 7.0]), and disrupted using low-temperature ultra-high pressure continuous flow cell disrupter. Bacterial solution was sedimented by centrifugation at 18 000 rpm at 4 °C for 40 min, and the supernatant was collected and purified using Ni Sepharose (GE) affinity chromatography following equilibration with buffer B (50 mM Tris, 300 mM NaCl [pH 7.0], and 20 mM imidazole). Proteins were eluted using buffer A supplemented with 250 mM imidazole. After concentration

by ultrafiltration and dilution in buffer C (50 mM Tris-HCl [pH 7.0]), the mixture was loaded onto a HiTrap Q 5 mL column (GE) pre-equilibrated with buffer C and eluted using a linear NaCl concentration gradient. The concentrated proteins were subjected to a final gel-filtration purification step on a Superdex 200 10/300 GL column (GE) in buffer D (50 mM Tris, 150 mM NaCl, [pH 7.0]). HiTrap Desalting 5 mL column (GE) was used to remove the salts from the purified proteins. The purity of the protein was verified on 15% SDS-PAGE gels. The resultant trifunctional protein was named as HGFI-TCS-smURFP (HTs).

Fluorescence Analysis of HTs: The fluorescence properties of smURFP and HTs were measured and compared. Solutions of smURFP and HTs were prepared at a concentration of 0.002 mg mL^{-1} (50 mM Tris, [pH 7]) and their absorption and emission properties were measured using an UV–vis spectrophotometer TU-90 and a fluorospectrophotometer F97XP, respectively. In total, 1 mL of protein sample was added into a colorimetric dish and tested according to the following conditions: absorption wavelength was detected from 500 to 700 nm and the emission wavelength of 600–750 nm was detected by fixing the excitation wavelength at 600 nm. Each measurement was repeated thrice and the obtained values were averaged.

WCA Measurement: The WCA of HTs was measured on hydrophobic polystyrene and hydrophilic mica sheets using an optical contact angle meter (KSV Instruments Ltd, CAM 200). In brief, a 0.2 mg mL^{-1} protein solution was prepared in sodium acetate-acetic acid buffer at pH 5.0 and 20 µL of it was dropped on the surface of polystyrene and mica sheets. After incubating the sheets at room temperature for 30 min, the protein solution was removed and the surfaces of the sheets were dried in a nitrogen stream. The HTs-modified surfaces were incubated at room temperature for overnight, and WCA was measured using a 5 µL water droplet on each modified surface. The contact angle was calculated as the average of the values obtained from at least three water drops.

Evaluation of the Functionality of the TCS Using ATPS: To verify the functionality of the thrombin restriction site, thrombin was added to the HTs solution (30 mg mL^{-1}) and the mixture was incubated at 37 °C for 20 min. ATPS analysis was carried out in a 1.5 mL volume of sample treated with 3% (M V^{-1}) Triton X-114. The two-phase system stood still and separated into two phases after about 20 min incubation at room temperature. Next, the fluorescence intensities of the upper buffer phase and the lower surfactant phase were measured at an excitation wavelength of 642 nm and an emission wavelength of 670 nm. The partition coefficient of smURFP in the two phases was calculated by dividing the fluorescence intensity from the surfactant phase by that from the buffer phase. The partition coefficients of HTs solution without thrombin and native smURFP in ATPS were measured and reported as control values.

Optimization of Immobilization of HTs on Multiwell Plates: The effects of pH and salt concentrations on the immobilization of HTs on multiwell plates were investigated. Buffers at different pH values (pH range from 3 to 10) were prepared. The buffers (10 mM) used included glycine-HCl (pH 3), sodium acetate-acetic acid (pH range from 4 to 6), monosodium phosphate-sodium hydroxide (NaH_2PO_4-NaOH; pH 7 and 8), glycine-NaOH (pH 9 and 10) buffers. These buffers were used to prepare a specific concentration of HTs (0.4 mg mL^{-1}). Next, 150 µL of HTs solution was added to the wells of a 96-well plate and the plate was incubated at 4 °C for overnight. After the removal of the residual liquid, the 96-well plate was washed thrice with 10 mM NaH_2PO_4-NaOH buffer (pH 7.4), and the fluorescence intensity was detected on an EnSpire Multilabel Reader. The same procedure was repeated for the evaluation of the effect of salt concentrations (sodium acetate, pH = 5, from 10 to 500 mM) on the immobilization of HTs on the multiwell plate. In addition, wash-resistant property (within seven rounds of washing) and stability of immobilized HTs (within a 15-day storage period at 4 or 37 °C) were also evaluated.

Characterization of HTs-Modified Polystyrene: The chemical composition of the HTs-modified and bare polystyrene surfaces was analyzed using an XPS apparatus (PHI-5300). XPS was performed to detect changes in the contents of C, N, O, and S elements on the surface of polystyrene. Bare polystyrene surface was used as a control. The source gun type was Al K Alpha, and the survey scan ranged from −9 to −1350 eV. All XPS spectra were recorded using an aperture slot of 400 × 400 µm; survey spectra were recorded at a pass energy of 150 eV, while high-resolution spectra were obtained at a pass energy of 30 eV.

The morphological changes in HTs-modified and bare polystyrene surfaces were also evaluated. In brief, 0.4, 0.6, and 0.8 mg mL^{-1} protein solutions were prepared (10 mM sodium acetate, pH = 5) and 20 µL of each solution was dropped onto the surface of polystyrene. The treated polystyrene was placed in a vacuum desiccator at room temperature for overnight. All samples were imaged in a dry state under the tapping mode using III Dimension 3100 AFM and silicon nitride cantilever at a nominal force constant of 50 N m^{-1} and scan rate of 1 Hz. The images from AFM were flattened to remove any possible tilt. Nova NanoSEM 430 was also used to observe the adsorption of fusion proteins on the surface of polystyrene. The high stability Schottky field emission gun was used as the source gun at an acceleration voltage of about 20 KV and a probe current of about 150 µA.

Thrombin Assay: After immobilization of HTs, thrombin at different concentrations was added to multiwell plates (from 1 aM to 1.07 mM, 10 mM Tris-HCl buffer [pH 7.4]). The plate was incubated at 37 °C for 20 min, and any residual liquid was removed by washing thrice with 10 mM NaH_2PO_4-NaOH buffer (pH 7.4). The fluorescence intensity was detected using EnSpire Multilabel Reader and compared with that reported before thrombin treatment. The difference was used to draw a standard curve. The above experimental steps were repeated in the presence of 20% human serum, human serum sample used in this study was purchased from Sigma-Aldrich. All the tests involved in the serum operation were proved by the Medical Ethics Committee of Tianjin University and strictly followed the biosafety regulation rules of Tianjin University.

The specificity of the detection system was verified. After immobilization of the same amount of HTs (150 µL) onto multiwell plates, 10^7 aM of different proteases (trypsin, elastase, chymotrypsin, proteinase K, thrombin, and 3 µM BSA in the presence of thrombin) were added to the multiwell plate; the above experiments were repeated. In brief, 3 µM BSA was mixed with thrombin to prove that the presence of high concentrations of other proteins had no effect on the fluorescence intensity associated with thrombin activity.

Statistical Analysis: Unless otherwise specified, all experimental data including: 1) fluorescence analysis of HTs; 2) WCA measurement; 3) evaluation of the functionality of the TCS using ATPS; 4) Optimization of immobilization of HTs on multiwell plates; and 5) thrombin assay were derived from three replicates. Error bars represent standard deviation. All numerical results were reported as mean ± SD, $n = 3$. In thrombin assay part, the linear equation was used to fit the data on HTs fluorescence and thrombin concentration by using Origin Lab software.

Supporting Information

Supporting Information is available from the Wiley Online Library or from the author.

Acknowledgements

H.Z. and L.Y. contributed equally to this work. Z.W. acknowledges the support of the National Natural Science Foundation of China (grant numbers 81601593 and 31970048). Y.W. acknowledges the support of the National Natural Science Foundation of China (grant number 61971302).

Conflict of Interest

The authors declare no conflict of interest.

Keywords

autofluorescence, far-red fluorescent proteins, hydrophobin, multifunctional proteins, self-assembly

Received: March 5, 2020
Revised: April 26, 2020
Published online:

[1] a) P. Fantl, M. Nance, *Nature* **1946**, *158*, 708; b) D. W. A. W, J. W. Lord Jr., J. T. Kauer, *Science* **1940**, *91*, 48.
[2] a) K. Y. Lin, G. A. Kwong, A. D. Warren, D. K. Wood, S. N. Bhatia, *ACS Nano* **2013**, *7*, 9001; b) T. Petzold, M. Thienel, I. Konrad, I. Schubert, R. Regenauer, B. Hoppe, M. Lorenz, A. Eckart, S. Chandraratne, C. Lennerz, C. Kolb, D. Braun, J. Jamasbi, R. Brandl, S. Braun, W. Siess, C. Schulz, S. Massberg, *Sci. Transl. Med.* **2016**, *8*, 367ra168.
[3] a) M. Sharma, *J. Am. Coll. Cardiol.* **2019**, *74*, 1924; b) H. A. de Silva, J. K. Aronson, D. G. Grahame-Smith, K. A. Jobst, A. D. Smith, *Lancet* **1998**, *352*, 1590.
[4] a) D. A. Gastineau, M. A. Gertz, T. M. Daniels, R. A. Kyle, E. J. Bowie, *Blood* **1991**, *77*, 2637; b) R. Sharma, A. P. Waller, S. Agrawal, K. J. Wolfgang, H. Luu, K. Shahzad, B. Isermann, W. E. Smoyer, M. T. Nieman, B. A. Kerlin, *J. Am. Soc. Nephrol.* **2017**, *28*, 2618.
[5] a) M. Badv, J. I. Weitz, T. F. Didar, *Small* **2019**, *15*, 1905562; b) M. A. Cavender, B. M. Scirica, M. P. Bonaca, D. J. Angiolillo, A. J. Dalby, M. Dellborg, J. Morais, S. A. Murphy, T. O. Ophuis, M. Tendera, E. Braunwald, D. A. Morrow, *Circulation* **2015**, *131*, 1047.
[6] a) J. P. Motta, A. Denadai-Souza, D. Sagnat, L. Guiraud, A. Edir, C. Bonnart, M. Sebbag, P. Rousset, A. Lapeyre, C. Seguy, N. Mathurine-Thomas, H. J. Galipeau, D. Bonnet, L. Alric, A. G. Buret, J. L. Wallace, A. Dufour, E. F. Verdu, M. D. Hollenberg, E. Oswald, M. Serino, C. Deraison, N. Vergnolle, *Nat. Commun.* **2019**, *10*, 3224; b) M. Z. Wojtukiewicz, D. Hempel, E. Sierko, S. C. Tucker, K. V. Honn, *Cancer Metastasis Rev.* **2016**, *35*, 213.
[7] P. Kongsuphol, S. K. Arya, C. C. Wong, L. J. Polla, M. K. Park, *Biosens. Bioelectron.* **2014**, *55*, 26.
[8] a) Y. Lin, Y. Sun, Y. Dai, W. Sun, X. Zhu, H. Liu, R. Han, D. Gao, C. Luo, X. Wang, *Talanta* **2020**, *207*, 120300; b) N. Yu, J. Wu, *Biosens. Bioelectron.* **2019**, *146*, 111726.
[9] a) T. Hao, X. Wu, L. Xu, L. Liu, W. Ma, H. Kuang, C. Xu, *Small* **2017**, *13*, 1603944; b) J. Li, W. Zhou, R. Yuan, Y. Xiang, *Anal. Chim. Acta* **2018**, *1038*, 126; c) X. Liu, X. Hua, Q. Fan, J. Chao, S. Su, Y. Q. Huang, L. Wang, W. Huang, *ACS Appl. Mater. Interfaces* **2015**, *7*, 16458; d) F. Cao, J. Chen, D. Yu, S. Wang, X. Xu, J. Liu, Z. Han, B. Huang, Y. Gu, K. L. Choy, H. Zeng, *Adv. Mater.* **2020**, *32*, 1905362.
[10] a) Y. Gao, Z. Zhu, X. Xi, T. Cao, W. Wen, X. Zhang, S. Wang, *Biosens. Bioelectron.* **2019**, *133*, 177; b) C. Zheng, A. X. Zheng, B. Liu, X. L. Zhang, Y. He, J. Li, H. H. Yang, G. Chen, *Chem. Commun.* **2014**, *50*, 13103.
[11] a) C. Ocana, M. del Valle, *Anal. Chim. Acta* **2016**, *912*, 117; b) V. Urbanova, K. Jayaramulu, A. Schneemann, S. Kment, R. A. Fischer, R. Zboril, *ACS Appl. Mater. Interfaces* **2018**, *10*, 41089; c) C. Zhu, W. Zhu, L. Xu, X. Zhou, *Anal. Chim. Acta* **2019**, *1047*, 21; d) S. Vasudevan, J. Kajtez, A. I. Bunea, A. Gonzalez-Ramos, T. Ramos-Moreno, A. Heiskanen, M. Kokaia, N. B. Larsen, A. Martinez-Serrano, S. S. Keller, J. Emneus, *Adv. Sci. (Weinheim, Ger.)* **2019**, *6*, 1902011; e) D. Ohayon, G. Nikiforidis, A. Savva, A. Giugni, S. Wustoni, T. Palanisamy, X. Chen, I. P. Maria, E. Di Fabrizio, P. Costa, I. McCulloch, S. Inal, *Nat. Mater.* **2020**, *19*, 456.
[12] a) X. Li, H. Kim, J. Litke, J. Wu, S. Jaffrey, *Angew. Chem., Int. Ed.* **2020**, *59*, 4511; b) P. Liu, E. W. Miller, *Acc. Chem. Res.* **2020**, *53*, 11.
[13] a) Z. Tao, X. Dang, X. Huang, M. D. Muzumdar, E. S. Xu, N. M. Bardhan, H. Song, R. Qi, Y. Yu, T. Li, W. Wei, J. Wyckoff, M. J. Birrer, A. M. Belcher, P. P. Ghoroghchian, *Biomaterials* **2017**, *134*, 202; b) Y. Zhao, F. Zheng, L. Shi, H. Liu, W. Ke, *ACS Appl. Mater. Interfaces* **2019**, *11*, 40669.
[14] H. Pakkila, S. Blom, K. Kopra, T. Soukka, *Analyst* **2013**, *138*, 5107.
[15] Y. Xiong, M. Liang, Y. Cheng, J. Zou, Y. Li, *Analyst* **2018**, *144*, 161.
[16] E. A. Rodriguez, G. N. Tran, L. A. Gross, J. L. Crisp, X. Shu, J. Y. Lin, R. Y. Tsien, *Nat. Methods* **2016**, *13*, 763.
[17] a) N. C. Shaner, R. E. Campbell, P. A. Steinbach, B. N. Giepmans, A. E. Palmer, R. Y. Tsien, *Nat. Biotechnol.* **2004**, *22*, 1567; b) J. H. Stack, M. Whitney, S. M. Rodems, B. A. Pollok, *Nat. Biotechnol.* **2000**, *18*, 1298; c) T. W. Chen, T. J. Wardill, Y. Sun, S. R. Pulver, S. L. Renninger, A. Baohan, E. R. Schreiter, R. A. Kerr, M. B. Orger, V. Jayaraman, L. L. Looger, K. Svoboda, D. S. Kim, *Nature* **2013**, *499*, 295; d) R. Y. Tsien, *Annu. Rev. Biochem.* **1998**, *67*, 509.
[18] W. R. Zipfel, R. M. Williams, W. W. Webb, *Nat. Biotechnol.* **2003**, *21*, 1369.
[19] a) L. Gazzera, R. Milani, L. Pirrie, M. Schmutz, C. Blanck, G. Resnati, P. Metrangolo, M. P. Krafft, *Angew. Chem., Int. Ed.* **2016**, *55*, 10263; b) H. Hahl, J. N. Vargas, A. Griffo, P. Laaksonen, G. Szilvay, M. Lienemann, K. Jacobs, R. Seemann, J. B. Fleury, *Adv. Mater.* **2017**, *29*, 1602888; c) A. M. Gravagnuolo, E. Morales-Narváez, S. Longobardi, E. T. da Silva, P. Giardina, A. Merkoçi, *Adv. Funct. Mater.* **2015**, *25*, 2771.
[20] a) A. M. Gravagnuolo, E. Morales-Narváez, C. R. S. Matos, S. Longobardi, P. Giardina, A. Merkoçi, *Adv. Funct. Mater.* **2015**, *25*, 6084; b) K. M. Bromley, R. J. Morris, L. Hobley, G. Brandani, R. M. Gillespie, M. McCluskey, U. Zachariae, D. Marenduzzo, N. R. Stanley-Wall, C. E. MacPhee, *Proc. Natl. Acad. Sci. U. S. A.* **2015**, *112*, 5419; c) I. Macindoe, A. H. Kwan, Q. Ren, V. K. Morris, W. Yang, J. P. Mackay, M. Sunde, *Proc. Natl. Acad. Sci. U. S. A.* **2012**, *109*, E804; d) Z. Wang, Y. Huang, S. Li, H. Xu, M. B. Linder, M. Qiao, *Biosens. Bioelectron.* **2010**, *26*, 1074.
[21] J. M. Kallio, M. B. Linder, J. Rouvinen, *J. Biol. Chem.* **2007**, *282*, 28733.
[22] A. Piscitelli, A. Pennacchio, P. Cicatiello, J. Politi, L. De Stefano, P. Giardina, *Biosens. Bioelectron.* **2017**, *87*, 816.
[23] a) D. Maiolo, C. Pigliacelli, P. S. Moreno, M. B. Violatto, L. Talamini, I. Tirotta, R. Piccirillo, M. Zucchetti, L. Morosi, R. Frapolli, G. Candiani, P. Bigini, P. Metrangolo, F. B. Bombelli, *ACS Nano* **2017**, *11*, 9413; b) B. N. Singh, B. R. Singh, V. K. Gupta, R. N. Kharwar, L. Pecoraro, *Trends Biotechnol.* **2018**, *36*, 1103.
[24] S. O. Lumsdon, J. Green, B. Stieglitz, *Colloids Surf., B* **2005**, *44*, 172.
[25] A. Collen, J. Persson, M. Linder, T. Nakari-Setala, M. Penttila, F. Tjerneld, U. Sivars, *Biochim. Biophys. Acta, Gen. Subj.* **2002**, *1569*, 139.
[26] Z. Wang, M. Lienemann, M. Qiau, M. B. Linder, *Langmuir* **2010**, *26*, 8491.
[27] R. Yamasaki, Y. Takatsuji, H. Asakawa, T. Fukuma, T. Haruyama, *ACS Nano* **2016**, *10*, 81.
[28] H. Wei, B. Li, J. Li, E. Wang, S. Dong, *Chem. Commun. (Cambridge, U. K.)* **2007**, *36*, 3735.
[29] H. Chang, L. Tang, Y. Wang, J. Jiang, J. Li, *Anal. Chem.* **2010**, *82*, 2341.
[30] A. Hecht, A. A. Kumar, R. Kopelman, *Anal. Chem.* **2011**, *83*, 7123.
[31] A. Trapaidze, J. P. Herault, J. M. Herbert, A. Bancaud, A. M. Gue, *Biosens. Bioelectron.* **2016**, *78*, 58.
[32] H. J. Chen, R. L. C. Chen, B. C. Hsieh, H. Y. Hsiao, Y. Kung, Y. T. Hou, T. J. Cheng, *Biosens. Bioelectron.* **2019**, *131*, 53.
[33] H. Kong, W. W. Liu, W. Zhang, Q. Zhang, C. H. Wang, M. I. Khan, Y. X. Wang, L. Y. Fan, C. X. Cao, *ACS Appl. Mater. Interfaces* **2019**, *11*, 29549.
[34] P. He, L. Liu, W. Qiao, S. Zhang, *Chem. Commun.* **2014**, *50*, 1481.

